International Journal of Railway Research, Vol. 4, No. 1, (2017), 13-27

Iran University of Science and Technology

International Journal of

Railway Research

ISSN: 2423-3838

A Numerical Study on Geofoam Application in the Settlement Reduction of Railway Embankments

Morteza Esmaeili[1*], Valiollah Khalilian[2], Fatemeh Khatibi[3]

[1,2,3]Iran University of Science and Technology, School of Railway Engineering, Tehran, Iran

ARTICLE INFO

Article history:
Received: 28.02.2017
Accepted: 8.05.2017
Published:17.06.2017

Keywords:
Geofoam
Railway embankment
Track settlement
Numerical analysis

A B S T R A C T

Construction of railway track embankment over a soft subgrade will bring the necessity of using soil improvement methods for bearing capacity and settlement criteria satisfaction. As a practical improvement method, railway embankment filled with geofoam blocks is studied in this paper. First a bilinear stress-strain model is developed in FLAC^{2D} to simulate geofoam embankment behavioral model. Second, the stability of a specified height range of geofoam embankments under static and dynamic train surcharges is investigated. Finally parametric studies are executed to monitor the variation of track dynamic settlement due to embankments height, subgrade un-drained strengths (Cu) and train surcharge amplitude and velocity. Results are verified. Such parameters can significantly affect the track dynamic settlement. Using multivariable regression and least squared methods analytical equations are derived to quantify an estimation of track dynamic settlement based on participating parameters

1. Introduction

Construction of a railway track over a soft subgrade can bring some difficulties due to providing enough bearing capacity and controlling short and long-term settlements. This can straightly lessen track maintenance intervals and increase the higher relevant costs. Soil improvement methods like compaction, injection, preloading, deep soil mixing and stone columns are solutions which are regularly used in such cases. Another method that has gained popularity in recent decades is making an embankment with light polystyrene material core that is usually called geofoam covered with soil. One of the main benefits of using geofoam blocks is to provide bearing capacity and controlling the embankment settlement is their small density. The usual order of geofoam weight per unit volume is almost 1% of soil's density. So, in case of high embankments, the self-weight of embankment is not a challenge. Fast construction process in comparison with other soil improvement methods is another benefit that has made this method more efficient.

Since 1960 different types of geofoam have been used for different civil projects and first usage as a geofoam embankment refers to 1985 in Japan.

In the field of research activities on stress-strain and creep behavior of this material, experimental studies have shown many factors including stress distribution, loading rate, temperature and moisture that can affect its stress-strain path, but the most determining factors are size and density.

In samples with a density around 18 kg/m^3 that experienced strains greater than 0.04, sample size have shown no effect on compressive strength (Trank and Erikson, 1991) [1]. Geofoam Poison's ratio has found to be a function of its density (i.e. increase with density increasing) (Japan, 1993) [2]. The stress-strain path of geofoam divided in to 4

*Corresponding author
Email address: m_esmaeili@iust.ac.ir
http:// tlx.doi.org/……..

[DOI: 10.22068/IJRARE.4.1.13]

parts including linear elastic, perfect plastic, linear strain hardening and nonlinear strain hardening (Horvath, 1995) [3].

Results of tests on creep behavior of 50 mm cubic samples of geofoam showed that creep displacement is negligible for samples which experienced less than 30% of compressive yield strength (Sun, 1997) [4]. Dynamic elastic modulus (E_d) of geofoam blocks is measured in the range of 4.7~6.1 MPa and 8.3~9.3 MPa for samples with 15kg/m^3 and 20kg/m^3 weight per unit volume, respectively (Duskov, 1997) [5]. Similar studies concluded that E_d will increase by density increase and also it's found to be negligibly affected by loading frequency. Geofoam damping ratio measured between 0.5% and 2% (Athanasopolos et al., 1999) [6]. A similar trend found between static elastic modulus (E_s) and density (Elragi, 2000) [7].

Determining the amount of elastic modules for different types of geofoam is a point of concern in many research studies. For small geofoam samples of type XIII, E_s measured almost 5Mpa according to ASTM C578 (Bartlett, 2000) [8] and for larger samples with same type E_s had measured more than14MPa (Elragi, 2000) [7]. Elastic modules determination for geofoam with curved structure is too complicated. Therefore, in these cases using laboratory and field experiments are inevitable. In order to consider the primary deflection due to gap closure between geofoam layers, the range of 2.3 to 2.7 MPa for E_s has been suggested (Negussey et al., 2001) [9]. The background and inspection conditions of EPS production in some countries and the homogeneous testing method that can examine the stability of EPS manufacturing procedure is described (Lee-Kuo et al., 2010) [10].

In the field of geofoam structural applicability, several research studies have been performed. Elastic modulus considering gap closures between blocks is measured in field studies (Newman et al., 2010) [11]. In the first stage of loading, the gap between blocks will be closed and in the second stage, blocks will go under compressive stress. Therefore, bilinear stress-strain diagram used as geofoam behavior model. Their model used for simulation of roadway embankment of Salt Lake City project.

The effect of geofoam compressible inclusion on lateral earth thrust acting on a rigid non yielding retaining wall was investigated by small-scale model tests and numerical analyses. Results of these studies showed significant reduction in the lateral earth pressures attributable to deformations concentrated at the lower half of retained soil mass (Ertugrul and Trandafir, 2011) [12].

EPS geofoam blocks have been used to provide a compensated foundation system for a single span bridge across Oatka Creek in Warsaw, NY (Stuedlein and Negussey, 2013) [13].

A combination of EPS geofoam and soil has been used to fill an excavation to ground level to support a roadway on grade (Anderson et al., 2013) [14].

A review on history of geofoam applicability in filling roadway excavation and bridge approach embankments, proves that geofoam have been brought enough satisfactory with design objectives.

Since encountering a soft subgrade in a railway track route is highly probable, it is important to find an efficient way for keeping the track settlement in the permitted range. Technical feasibility of geofoam railway embankments as a solution in such cases is investigated in this paper. The main objective is to study the effect of geofoam core on train passing dynamic settlements of railway embankment. For this purpose, a script coding in FLAC^{2D} is used to develop geofoam behavioral model. The validity of behavioral model is calibrated by field measurements and numerical works of Newman et al., 2010. Then geofoam embankment stability analysis under static and dynamic loads is performed using Slide software and desired geofoam type is chosen based on ASTM suggestions for each static stress level. Finally, the finite difference method is used to model track fills with different heights over soft to medium clay subgrades. Models are analyzed under train dynamic surcharges representing different track axle loads with varying velocities. Track dynamic settlement based on participating parameters is quantified using multivariable regression and least squared methods.

2. Geofoam Type Selection for Engineering Design

Geofoam blocks have been used in several road projects as filling material. In this study, the applicability of these blocks in case of railway track embankment is investigated. Figure 1 shows a schematic section of such a track embankment. As it is illustrated in Figure 1, geofoam blocks are used as the embankment core and are covered with a lining layer and coating soil. Over the top lining layer the track pavement which is a concrete slab is constructed.

Since the determinant stress that the embankment experiences during the rail operation

[DOI: 10.22068/IJRARE.4.1.13]

is compressive, geofoam blocks should satisfy enough compressive strength against passing loads

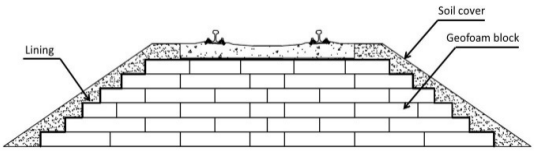

Figure 1. Schematic section of geofoam railway embankment

and also provide the serviceability criteria. As an obvious phenomenon, with going through the depth of embankment, stress will be dissipated. It means that at different depth of embankment, different types of geofoam can satisfy serviceability requirements. The main factor for choosing the type of geofoam, based on its engineering properties, is the stress intensity level. The total amount of stress at each depth of embankment, σ_z, is calculated by the procedure that is suggested by Stark et al., 2004 as in Equation (1):

$$\sigma_z = \sigma_{z,LL} + \Delta\sigma_{z,DL} + (\gamma_g . z) \quad (1)$$

where, $\sigma_{z,LL}$ is the stress due to train traffic load. If the stress intensity assumed to dissipate through the embankment depth by theoretical 1:2 (V:H) method, then Equation (2) can be used to calculate $\sigma_{z,LL}$ at each arbitrary depth of z. Q represents the embankment surcharge in this relation and dimensions of surcharge distribution rectangle are noted as B and L.

$$\sigma_{z,LL} = \frac{Q}{(B+z)(L+z)} \quad (2)$$

$\Delta\sigma_{z,DL}$ is the extra stress due to railway pavement weight and is calculated according to Equation (3):

$$\Delta\sigma_{z,DL} = \left(\frac{q}{\pi}\right)(\alpha + sin\alpha)$$
$$\alpha = 2tan^{-1}(\frac{b}{z}) \quad (3)$$

where q is surface pressure and b is the half width of the pavement as is illustrated in Figure 2. γ_g is the geofoam density that multiplying to z, will give the geofoam weight at each depth.

Standard train loading pattern of LM71 which is shown in Figure 3 is used for applying on the embankment surface. Different axial loads of 150, 200 and 250 KN are used as surcharge amplitude.

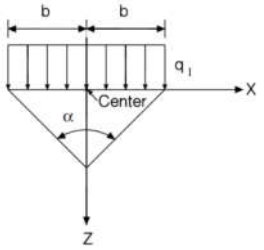

Figure 2. Variables needed to calculate extra stresses induced by dead load in depth z (Stark et al., 2004)

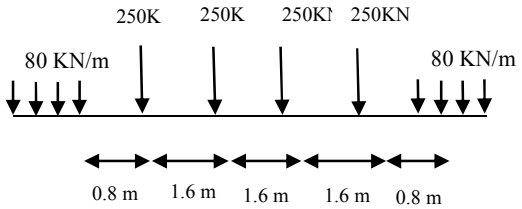

Figure 3. Train vertical load model UIC71

In order to develop a plane strain model, load per 1.6 meter length of track plus slab track pavement (0.4 m height and 25 kN/m^3 density) weight is calculated and distributed over a 3.1 m top width of embankment section. Figure 4 shows the schematic embankment assumed for this calculation.

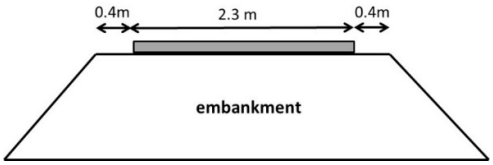

Figure 4. Schematic of railway embankment section

The impact factor presented in Arema, 2006 (Equation (4)) is used to gain total pressure on the fill surface under different axle loads and different speeds:

$$\alpha = 1 + 5.21(V/D) \quad (4)$$

where V is train velocity in Km/h and D is train wheel diameter that is equal to 1000 mm. For determining the stress value at each depth, appropriate geofoam type is selected according to ASTM C578 for each desired depth. Geofoam types which are selected by this method are presented in Table 1. (i.e. for axle load of 250KN, stress at depths between 0 to 2.5 m is 96.92 KPa

[DOI: 10.22068/IJRARE.4.1.13]

Table 1. Total stresses and suggested geofoam type based ASTM, C578

Z (m)	V (Km/h)	α	Train axle load (KN)					
			150		200		250	
			Stress (kPa)	Geofoam type	Stress (kPa)	Geofoam type	Stress (kPa)	Geofoam type
0-2.5	120	1.6252	64.15	I	80.53	VIII	96.92	XII
	240	2.2504	83.06	VIII	105.74	IV	128.43	IV
	360	2.8756	101.96	XII	130.95	IV	159.94	IV
2.5-5	120	1.6252	55.85	I	70.11	VIII	84.37	VIII
	240	2.2504	72.31	VIII	92.06	XII	111.81	IV
	360	2.8756	88.77	VIII	114.00	IV	139.24	IV
5-7.5	120	1.6252	40.08	I	50.32	I	60.56	I
	240	2.2504	51.90	I	66.07	I	80.25	VIII
	360	2.8756	63.71	I	81.82	VIII	99.94	XII
7.5-10	120	1.6252	29.63	XI	37.20	I	44.76	I
	240	2.2504	38.36	I	48.84	I	59.32	I
	360	2.8756	47.09	I	60.48	I	73.87	VIII
10-12.5	120	1.6252	23.14	XI	29.04	XI	34.95	XI
	240	2.2504	29.95	XI	38.14	I	46.32	I
	360	2.8756	36.77	I	47.23	I	57.68	I

and appropriate geofoam type is XII).

The schematic section of 12.5 m embankment analyzed under 250 KN train axle load at different speeds is illustrated in Figure 5.

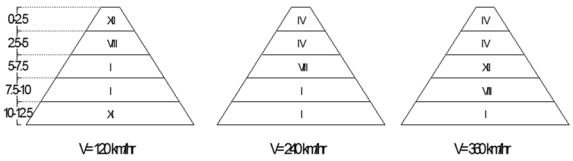

Figure 5. Schematic section of 12.5m height embankments analyzed under 250KN axle load

3. Constitutive Model Development for Geofoam Embankment

The behavioral model of a group of geofoam blocks which are set in rows over each other different from a single geofoam block. When layers of geofoam blocks experience a compressive stress, first blocks will deform to fill narrow spaces between rows. After this gap closuring stage completed and seals between blocks disappeared, the mechanical properties of single block would determine the stress-strain response of material. Since these two stages can be detected in compressive response of layers of geofoam blocks, the behavioral model of a geofoam embankment cannot be assumed according to stress-strain path of a geofoam material as well. Newman et al. (2010), derived out the elastic modulus of geofoam embankment. Considering gap closures between blocks, in the primary seconds after loading proceeding by geofoam strains, they suggested a bilinear stress-strain diagram like Figure 6 for EPS geofoam embankment. As it is illustrated in Figure 6, up to stress level of 15KPa, where vertical strains are due to gap closure, elastic modulus is denoted by E_0. Newman et al. (2010), assumed low stress modules including 1.7, 2.3 and 2.7 MPa for E_0 and developed a model based on each assumption. By increasing the compressive stress, the elastic modulus of geofoam material, E_1 would work as the elastic modulus of whole embankment.

In this paper a stress-strain path is developed using FISH programming language in FLAC^{2D} package. In this model E_0 is assumed as equal to 2.7 MPa and E_1 is changed by geofoam type that is selected according to stress level. The developed model is verified by comparing vertical displacement and stresses of

[DOI: 10.22068/IJRARE.4.1.13]

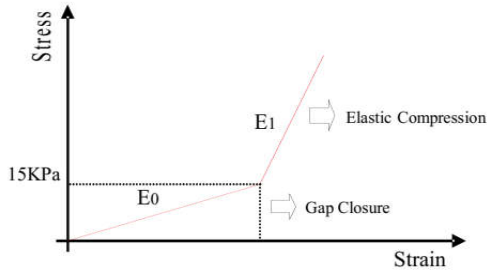

Figure 6. Geofoam blocks stress-strain model

embankment with results of Salt Lake City project.

The cross section of EPS road embankment of Salt Lake City project are divided to five monitoring points denoting by level0, level6, level9, LDS and UTBC. In addition to field measurements at those five layers, the mentioned road embankment was numerically simulated by Newman et al, (2010). Material properties that are used in their analysis and are also used in the stage of behavioral model calibration in this paper are according to Table 2.

Figure 7 illustrates the geometry of EPS embankment of Salt Lake City project that is generated in FLAC^{2D} to verify the behavioral model

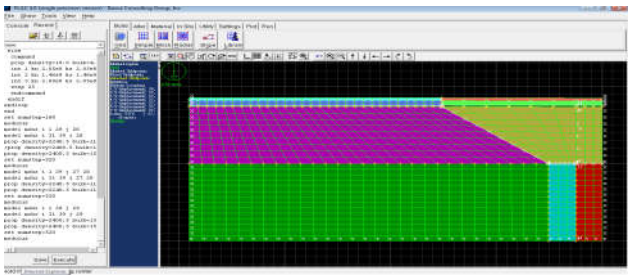

Figure 7. Primary model in FLAC, used for calibration

Vertical stress and displacement results of Salt Lake City embankment simulation in FLAC software are mapped by red line according to the diagrams by Newman et al. (2010). Results are presented in Figures 8 and 9, respectively.

The good agreement between red curve data and other curves is a clear evidence that behavioral model validity can be assumed to be admitted.

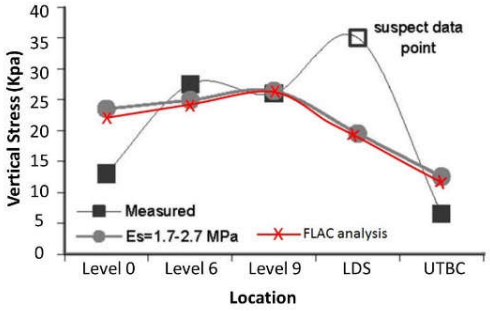

Figure 8. Behavioral model calibration using vertical stress data (Adapted from Newman et al., 2010 [11])

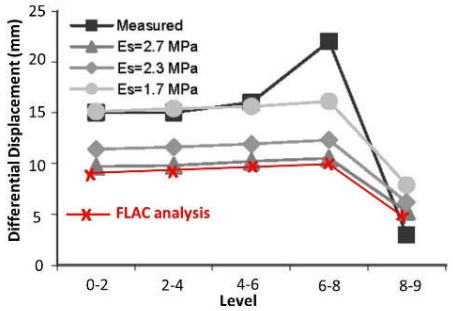

Figure 9. Behavioral model calibration using vertical displacement data (Adapted from Newman et al., 2010 [11])

This calibration, also admits correct usage of software. All other models in this paper are generated in same way.

4. Static Numerical Analysis of Geofoam Railway Embankment

Before studying the serviceability of geofoam railway embankment under train dynamic loads, weight per unit volume of different parts of model is assigned and gravity is turned activated to analyze the model to reach initial equilibrium state. Also a 2D model of embankment is developed using Slide software. Stability of geofoam embankments with different heights from 2.5 to 12 m are investigated. In the following, the modeling procedure and characteristics are described in more details.

[DOI: 10.22068/IJRARE.4.1.13]

Table 2. Material properties for numerical models (Newman et al., 2010)

Material	Kg/m^3)(**ρ**	**υ**	**E**(MPa)	**K**(MPa)	**G**(MPa)	Ø (°)	**C**(MPa)
Pre-existing soil Base sand underlying soil	2160	0.35	100	111	37	35	0
Geofoam σ ≤ 15 KPa	18	0.103	1.7-2.7	0.714-1.13	0.771-1.22	35	0.005
Geofoam σ ≥ 15 KPa			10	4.20	4.53		
LDS	2400	0.18	30000	15600	12700	25	25
PCCP							
UTBC	2240	0.35	100	111	37	35	0

4.1. Material model

The whole model is made up of three different parts including track pavement, embankment body and clay subgrade top-down, respectively. The slab track system is selected for track pavement as it more agrees to geofoam embankment structure than ballast track. Therefore, the mechanical properties of concrete and a linear elastic model are assigned to the generated mesh part at the top of embankment to represent slab track pavement system. As it is mentioned in section 2, geofoam type selection at each depth is dependent to stress level the embankment is going to experience. EPS Geofoam types, including I, XI, VIII and XII, according to ASTM C578, are assigned to different layers of the zone representing the embankment body. Material behavioral model for this part is the bilinear elastic model that is developed and calibrated based on Newman et al., model.

Soft to medium clay soils with un-drained strengths range between 20 to 60 kPa considered for modeling subgrade layer in different analysis. According to semi empirical formulation of Bjerrum (1972) elastic modulus of clay layer can be assumed by following equation:

$$Eu=500xCu \quad (5)$$

where cu is the un-drained shear strength determined from a field vane shear test. This relation gives a rough estimate of Eu and is appropriate for highly plastic clays. Mechanical properties and constitutive models for each material part are presented in Table 3.

4.2. Geometry and boundary conditions

Figure 10 illustrates the general geometry used to generate desired models. The upper width of embankment as illustrated in Figure 4 is taken as 3.1 m. Embankment height is assumed to take values of 2.5, 5, 7.5, 10 and 12.5 m. The side slope of fills is selected 1:1.5 (V:H) according to stability analysis results of Slide software. The dimensions of subgrade layer are selected large enough to make fixed boundaries assumption possible.

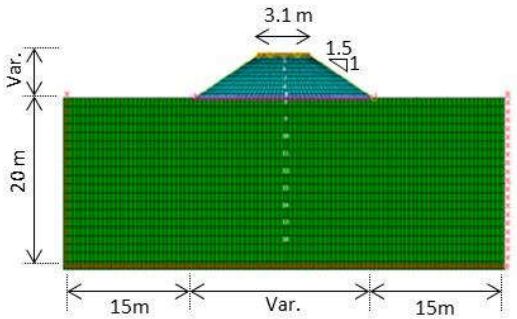

Figure 10. Embankment with 5 m height model in FLAC^{2D}

The bottom horizontal boundary of subgrade is fixed at both X and Y directions. Vertical boundaries at both sides of subgrade layer and the

[DOI: 10.22068/IJRARE.4.1.13]

Table 3. Geotechnical parameters used for numerical modeling of pavement, embankment and subgrade, in FLAC

Material		C (kPa)	Φ (°)	γ (kg/m³)	υ	E (MPa)		G (MPa)	K (MPa)	Constitutive model
		cohesion	friction angle	density	Poisson ratio	Young's modulus		shear modulus	bulk modulus	
Concrete slab		-	-	2500	0.18	21000		12712	15625	elastic
Geofoam Embankment	XII	25	30	19	0.109	E_0	2.7	1.217	1.151	Strain hardening
						E_1	10	4.508	4.263	
	VIII			18	0.103	E_0	2.7	1.224	1.134	
						E_1	9	4.079	3.780	
	I			15	0.086	E_0	2.7	1.242	1.088	
						E_1	6.5	2.991	2.619	
	XI			12	0.069	E_0	2.7	1.262	1.045	
						E_1	4	1.869	1.548	
Clay Subgrade		20	1	1700	0.4	500xC_U		3.57	16.67	Mohr-Columb
		25						4.46	20.84	
		30						5.36	25	
		35						6.25	29.17	
		40						7.14	33.34	
		45						8	37.5	
		50						8.93	41.67	
		55						9.82	45.84	
		60						10.7	50	

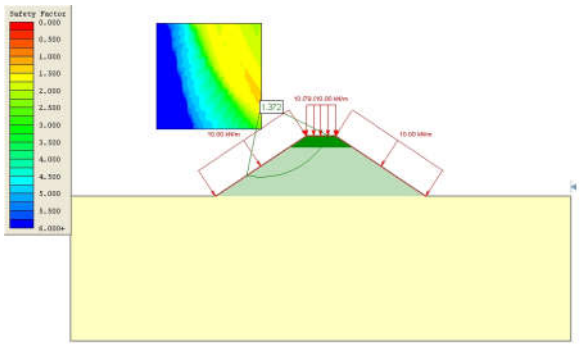

Figure 11. Stability control under static surcharges Slide

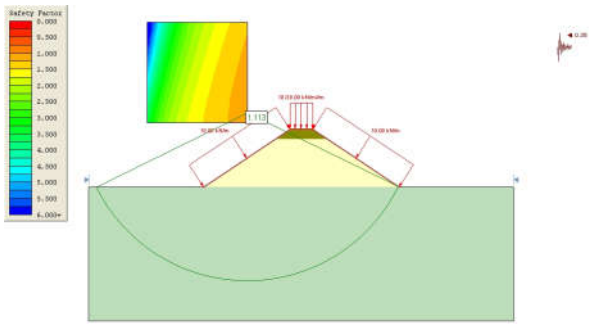

Figure 12. Stability control under dynamic surcharges Slide

[DOI: 10.22068/IJRARE.4.1.13]

horizontal interface between embankment and subgrade are only fixed at X direction. All other boundaries are free surfaces.

4.3. Stability control results

In order to determine the side slope of geofoam fills, stability analysis under three different situations described below, are performed in Slide software.

1- Short-term stability under static loads

2- Long-term stability under static loads

3- Stability under earthquake loads

Static load model of UIC71 is used as loading pattern and for each analysis; the heaviest axle load in the pattern is distributed as a line load and applied on the crest line of embankment. Table 4 shows the amounts of required safety factor for embankment in these three cases, according to different standards

Results of static and dynamic stability control of 12.5 m height embankment are illustrated in Figures 11 and 12, respectively.

The satisfactory of side slope equal to 1:1.5 (V:H) is admitted for all embankments that are considered for this research.

4.4. Model generation and initial equilibrium state

After the stability control of embankment showed enough safety factors against sliding and satisfaction of model geometry condition, weight analysis of model performed to reach initial equilibrium. The subgrade layer is developed by ten stages of filling. In each step, 2-m filling based on elastic behavior analyzed and after getting equilibrium condition all displacements set to zero and the next stage proceeded accordingly. Then the soil behavioral model prior to loading the system is changed from elastic to the Mohr–Columb model. After the generation of subgrade completed, different layers of embankment modeled by elastic behavior.

Figure 13 and 14 illustrate normal stresses and displacement contours of the 5 m height embankment.

Table 4. Embankment stability safety factor according to different standards

standard	type	Static loading		earthquake	description
		Short-term	Long-term		
FHWA-NHI-00-043	MSEW	1.5		1.125	Mechanical stabilized earth wall
	RSS	1.3		0.975	Reinforced soil slope
FHW A0-IF-03-017	Nailing Wall (tempo structure)	1.35		1.1	Geotechnical engineering circular no. 7- soil nail walls
	Nailing Wall (perma structure)	1.5		1.1	-
AREMA	-	1.5		-	-
U.S. army corps	End of construction	1.25		1	stability of earth and rockfill dams EM 1110-2-1902
A.S.C.E	End of construction	1.3		1	S(slow- CD) or Q(Quick - UU)
A.S.C.E. (Recommendation procedures for implementation of dmg special publication 117)	-	1.25	1.5	1	-

[DOI: 10.22068/IJRARE.4.1.13]

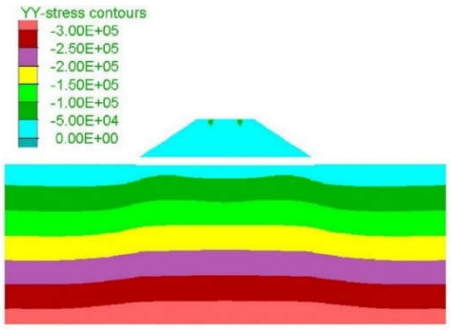

Figure 13. Normal stress contours under model weight

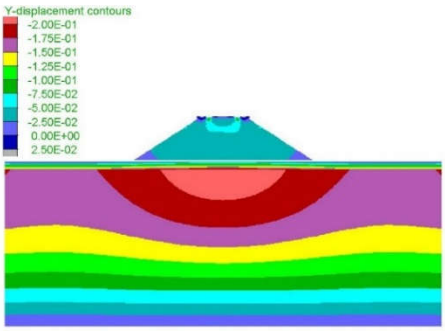

Figure 14. Normal displacement contours under model weight

After initial equilibrium state achieved, bilinear elastic model is assigned to embankment and dynamic analysis are executed.

5. Dynamic Analysis of Geofoam Railway Embankment

After the stability of embankment is admitted and the initial equilibrium state is achieved, the dynamic loads representing train surcharges at different speeds are applied on the embankment and dynamic analysis are executed. The main objective to perform dynamic analysis stage is to investigate how the geofoam core of the generated railway embankment can affect track settlement trend in case of existence of a soft or medium clay subgrade. In dynamic analysis, the geometry and boundary conditions in model are the same as the static analysis. Based on dynamic load frequency, both embankment and subgrade zones are divided with 0.5x1 m rectangular mesh parts. Because of dynamic nature of loading, damping ratios equal to 0.5% and 5% assigned to geofoam embankment and clay subgrade zones, respectively. Local damping model used to assign these values.

The elastic modulus of subgrade soil is taken 1.5 times greater than static value to represent a better approximation of subgrade response in dynamic condition (E_{dy}= 1.5 E_{st}). Train surcharge is approximated by the harmonic formulation of following relation:

$$F = P\left(1 - Cos(2\pi f t)\right) \quad (6)$$

where P is amplitude of train axial load, f is load passing frequency and t represents time. Load passing frequency is according to the following equation:

$$f = \frac{V}{L} \quad (7)$$

where V represents train velocity and L is bogies center to center distance that is considered 18.7 m according to Thalys train wagon configuration. In dynamic analysis, train speed changed from 100 to 350 km/h. Frequency and speed values that are used in dynamic analysis are presented in Table 5.

Table 5. Frequency range used to in dynamic analysis

V(km/h)	100	150	200	250	300	350	
f (sec^{-1})	1.48	2.23	2.97	3.71	4.45	5.2	

As it is described in section 2, static loading amplitude used in geofoam type selection is the heaviest train axle load in LM71 pattern which is distributed as compressive stress over the embankment. These axle loads are used as harmonic load amplitudes in dynamic analysis.

[DOI: 10.22068/IJRARE.4.1.13]

According to different variable parameters in analyzing, such as loading, un-drained strength of subgrade, embankment height, geofoam type and train passing velocity, 450 different versions of model have been developed and analyzed. The analysis time is taken long enough to consider passing the whole 100 m train over the embankment.

6. Results and Discussion

Dynamic Settlement of railway embankments under axial loads of 150, 200 and 250 kN and train velocities from 100 to 350 km/hr are investigated. Geofoam embankment height changed from 2.5 to 12.5 m and un-drained strength of subgrade varies from 20 to 60 KPa. Settlement results at the track center point just beneath the slab track zone in the model are extracted. Figure 15 illustrates how the amount of track settlement changed with train normalized speed under 250kN axial load.

As a natural result, by increasing the un-drained strength of subgrade, less amount of settlement is occurred. The difference between curves belonging to different subgrades is decreased as the embankment height is increased, and in case of embankments with 10 and 12 m height, the calculated settlement curves are nearly overlapped. That means by increase in embankment height, the effect of subgrade strength on track vertical displacement is disappeared and settlement is mostly controlled by embankment material.

Despite the 12.5 m height embankment that shows a minimum point at the normalized velocity of 2.4, in other embankments increasing the train normalized velocity a decreasing trend in the amount of settlement can be detected. That means at higher train velocities geofoam core is more efficient for settlement control. There is an exception in the described manner that is regarded as increase in settlement of embankment with 12.5 m height, between 2.4 and 3.6 normalized velocities. Because the only difference between this exception case and other graphs of Figure 15 is the height of embankment, it can be concluded that for efficient operation of geofoam blocks as settlement controlling materials in railway embankments, a height threshold boundary existed.

Track Settlement curves under 200 and 150 KN train axle loads are illustrated in Figures 16 and 17, respectively. Settlement values are decreased in comparison to Figure 15, regarding to decrease in the train axle load. The minimum point that could be detected only in settlement curves of diagram (a) of Figure 15, is appeared in diagrams (a), (b) and (c) of Figures 16 and 17.

It means that by decrease in harmonic load amplitude, the mentioned height threshold is decreased. Many more analysis with varying values of train axial load and velocities on railway embankments with different conditions need to be executed to reach an accurate judgment about this threshold height and efficient operation of geofoam blocks as railway embankment core.

Considering the settlement permitted value in railway standards, presented graphs of Figures 16 to 17 can be referenced for primary estimation of safe train velocities in case of different axle loads.

In order to quantify a primary estimation of dynamic settlement based on three parameters including embankment height, train velocity and train axle load, multivariable regression and least square method are used. Basic equation is according to following formulation:

$$Y = f(X_1, X_2, X_3, X_4) \quad (8)$$

$$Y = \alpha . {X_1}^{\beta} . {X_2}^{\gamma} . {X_3}^{\eta} . {X_4}^{\zeta} \quad (9)$$

where Y is dynamic settlement and denotes with S_{dy}, $X_1 = \frac{P}{250}$ in which P is train axial load in Kilo Newton, X_2 is embankment height (H), $X_3 = \frac{E_G}{E_{sub}}$ and X_4 is normalized velocity ($\frac{V}{100}$). In this relation, Y, X_1, X_2, X_3 and X_4 are equation parameters and α, β, γ, η and ζ are unknown values to determine. Therefore, Equation (9) can

[DOI: 10.22068/IJRARE.4.1.13]

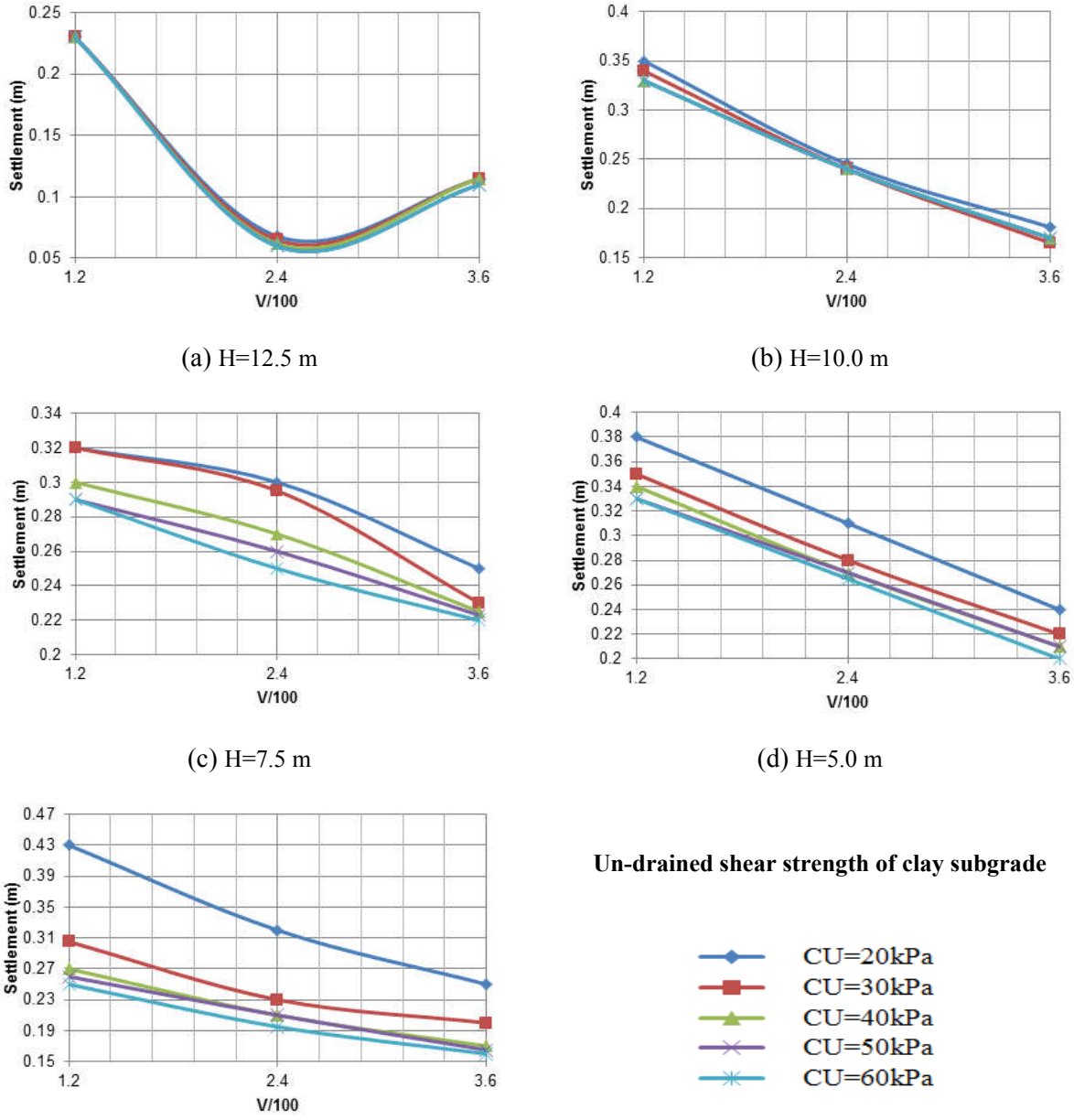

Figure 15. Dynamic Settlement of geofoam embankment under 250 KN axle load

[DOI: 10.22068/IJRARE.4.1.13]

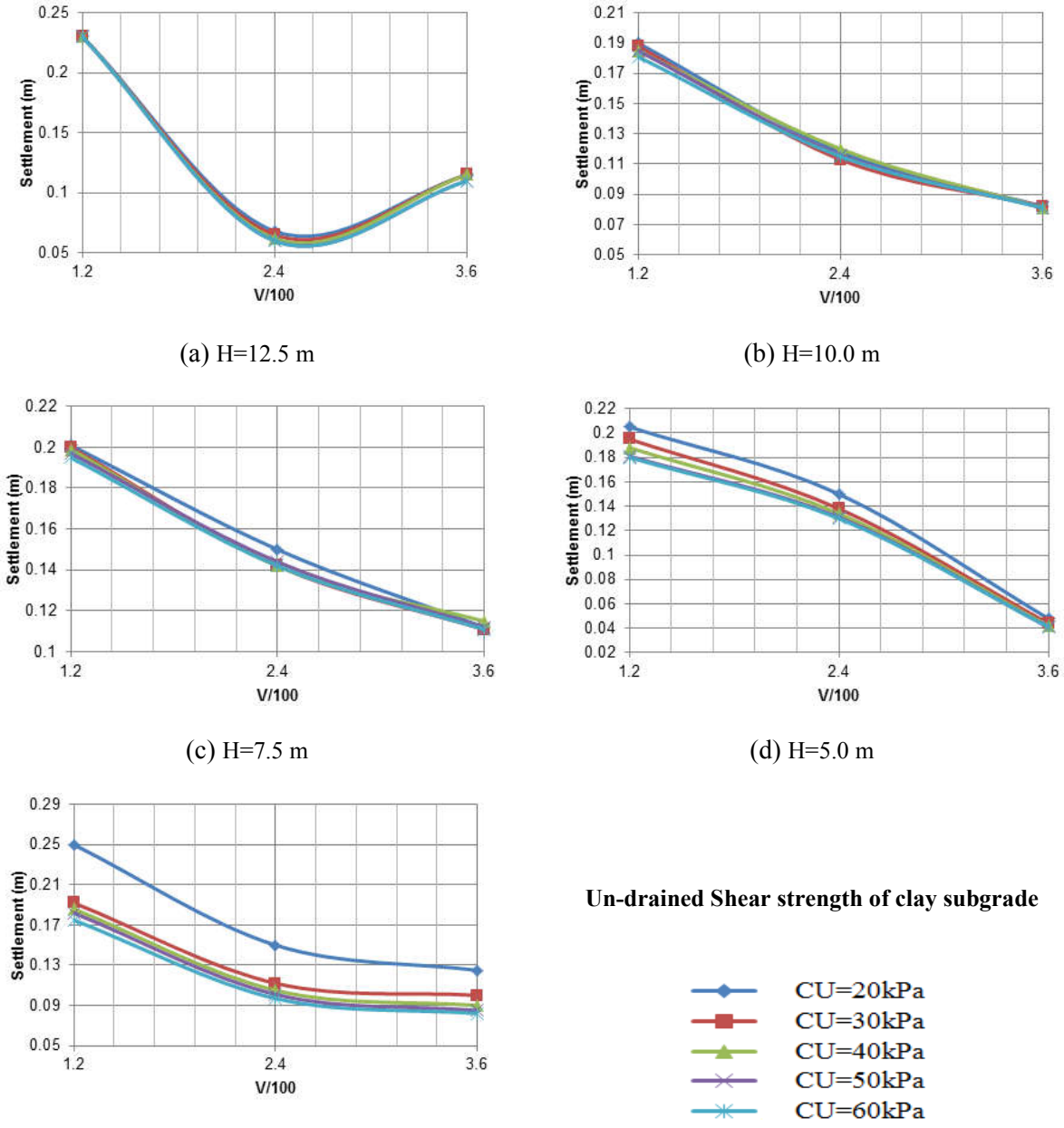

Figure 16. Dynamic Settlement of geofoam embankment under 200 KN axle load

[DOI: 10.22068/IJRARE.4.1.13]

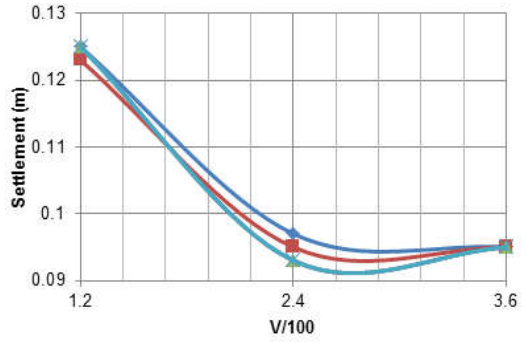

(a) H=12.5 m

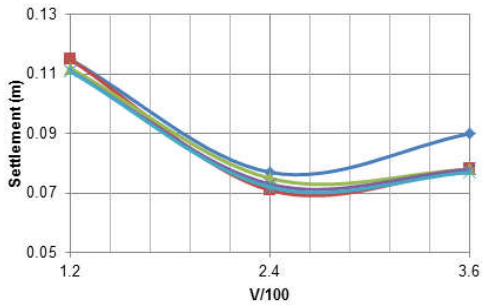

(b) H=10.0 m

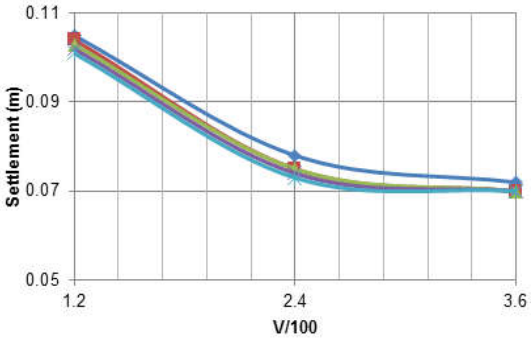

(c) H=7.5 m

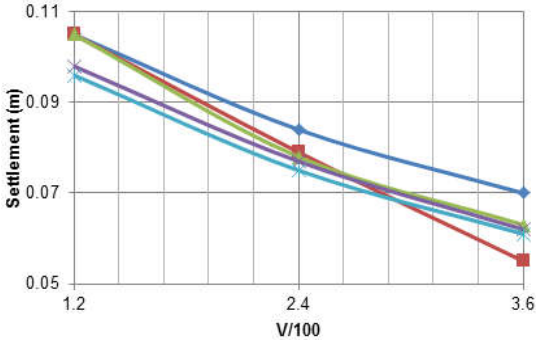

(d) H=5.0 m

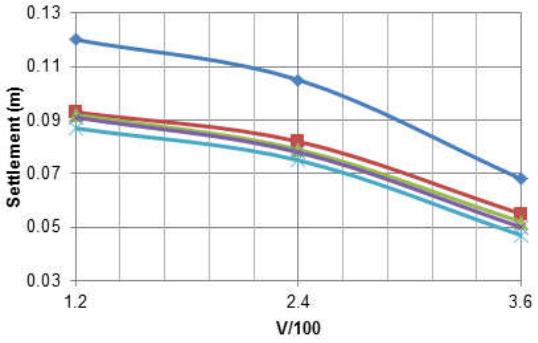

(e) H=2.5 m

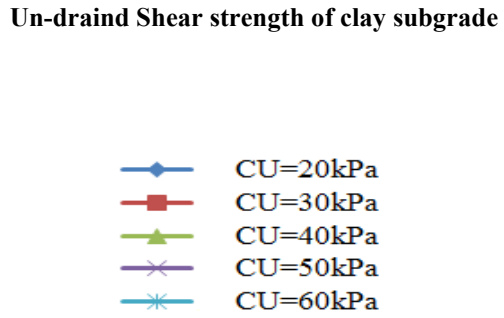

Figure 17. Dynamic Settlement of geofoam embankment under 150 KN axle load

[DOI: 10.22068/IJRARE.4.1.13]

be rewritten as follows:

$$S_{dy} = \alpha.\left(\frac{P}{250}\right)^{\beta}.H^{\gamma}.\left(\frac{E_G}{E_{sub}}\right)^{\eta}.\left(\frac{V}{100}\right)^{\zeta} \quad (10)$$

Using least square method unknown values are obtained and dynamic settlement equation is:

$$S_{dy} = 0.355\left(\frac{P}{250}\right)^{1.736}.H^{-0.008}.\left(\frac{E_G}{E_{sub}}\right)^{0.094}\left(\frac{V}{100}\right)^{-0.566} \quad (11)$$

Comparing settlement results between least square method and finite difference process in FLAC showed that the accuracy with the least square method is around 0.98.

7. Conclusions

Considering the successful usage of geofoam blocks in road projects, the applicability of geofoam blocks in the serviceability improvement of railway embankment is investigated. Track geofoam embankment with different heights over soft to medium clay subgrades analyzed numerically in FLAC^{2D}. Dynamic surcharges applied on plane strain model and dynamic settlements are calculated. Main results of this study are summarized here:

- Dynamic settlement of geofoam embankment will decrease, by increasing undrained strength of subgrade.
- Reducing the embankment height and axle load will decrease dynamic settlement.
- By increasing the embankment height, the amount of dynamic settlement will be affected mostly by embankment material and subgrade participation will be decreased.
- In case of embankments with equal or less than 5 m in height, by increasing the train normalized velocity, dynamic settlement will be decreased.
- In case of embankments with more than 5 m height, depending on the axial load, dynamic settlement will decrease by increase in normalized velocity up to 2.4 and then will be increased.
- In order to estimate settlement of geofoam embankment under dynamic surcharge, use of Equation (11) that is presented in this article is suggested.

References

[1] L. Eriksson and R. Trank, Properties of expanded polystyrene, Laboratory Experiments, Swedish Geotechnical Institute, Linköping, Sweden, (1991).

[2] EPS, Expanded polystyrol construction method development organization, Tokyo, Japan, (1993), 310 pp.

[3] J.S. Horvath, Geofoam Geosynthetic, Horvath Engineering, P.C., Scarsdale, NY, (1995), 229 pp.

[4] M.C. Sun, Engineering behavior of geofoam (expanded polystyrene) and lateral pressure reduction in substructures, Master Thesis, Syracuse University, New York, (1997).

[5] M. Duskov, Material research on EPS-20 and EPS-15 under representative conditions in pavement structure, Geotextiles and Geomembranes, Vol. 15, No.1, 2, and 3, (1997), pp. 147-181

[6] G.A. Athanasopoulos, P.C. Pelekis and V.C. Xenaki, Dynamic properties of EPS geofoam, Graduate Student, Department of Civil Engineering, University of Patras, (1999), Greece.

[7] A. Elragi, Selected engineering properties and applications of EPS geofoam, Ph.D. Thesis, State University of New York, Syracuse, N.Y., (2000).

[8] S. Bartlett, D. Negussey, M. Kimble and M. Sheeley, Use of geofoam as super-lightweight fill for I-15 reconstruction. Proc., Transportation Research Board 79th Annual Meeting, Transportation Research Board, Washington, D.C., (2000).

[9] D. Negussey, A.W. Stuedlin, S.F. Bartlett and C. Farnsworth, Performance of geofoam embankment at 100 South, I-15 reconstruc project, Salt Lake City, Utah. Proc., EPS Geofoam, 3rd Int.Conf. Salt Lake City, Utah, 22, (2001).

[DOI: 10.22068/IJRARE.4.1.13]

[10] L. Lee-Kuo, C. Li-Hsien and H.L. Roger, Evaluation of geofoam as a geotechnical construction material, Journal of Materials in Civil Engineering, Vol. 22, No. 2, (2010), 160-170.

[11] M.P. Newman, S.F. Bartlett and E.C. Lawton, Numerical modeling of geofoam embankments, Journal of Geotechnical and Geoenvironmental Engineering, Vol. 136, No. 2, (2010), pp. 290-298

[12] O.L. Ertugrul and A.C. Trandafir, Reduction of lateral earth forces acting on rigid nonyielding retaining walls by EPS geofoam inclusions, Journal of Materials in Civil Engineering, Vol. 23, No. 12, (2011), pp. 1711-1718

[13] A.W. Stuedlein and D. Negussey, Use of EPS geofoam for support of a bridge, Sound Geotechnical Research to Practice Honoring Robert D. Holtz, Geotechnical Special Publication No. 230, ASCE, Reston, VA., (2013), pp. 334-345.

[14] J. Anderson, P. Poepsel and K. Kriete, Design and construction of free standing expanded polystyrene roadway embankment in downtown St. Louis, Missouri, Geo-Congress, (2013), pp. 1429-1438.

[15] ASTM, Standard specification for rigid, cellular polystyrene thermal insulation, Developed by Subcommittee: C16.22, Active Standard ASTM C578.

[DOI: 10.22068/IJRARE.4.1.13]